Zero Voltage Vector Selection in a Saturation Controller-Based Direct Torque Control for Permanent-Magnet Synchronous Motors

Lizhi Qu, Liyan Qu, and Wei Qiao
Power and Energy Systems Laboratory
Department of Electrical and Computer Engineering
University of Nebraska−Lincoln
Lincoln, NE 68588-0511 USA
lizhi.qu@huskers.unl.edu; lqu2@unl.edu; wqiao3@unl.edu

Zhe Zhang
Machine Systems Technology, Eaton Research Labs
Eaton Corporation
Southfield, MI 48076 USA
Zhezhang1@eaton.com

***Abstract*—This paper analyzes the effect of zero voltage vectors on the torque and stator flux of a direct torque controlled salient-pole permanent-magnet synchronous motor (PMSM). Four different schemes of using the zero voltage vectors are studied for an adaptive saturation controller-based direct torque control (DTC) system for salient-pole PMSMs. The four schemes generate four different pulse-width modulation (PWM) waveforms in each control cycle of the DTC system, which are three-voltage-vectors-based minimum discontinuous PWM (DPWMMIN), maximum discontinuous PWM (DPWMAX), and discontinuous PWM (DPWM), and four-voltage-vectors-based continuous PWM (CPWM). Compared to the DPWMMIN, DPWM, and DPWMMAX, the CPWM can achieve a lower torque ripple, less steady-state torque error, and more sinusoidal stator current with a higher switching frequency and, therefore, has a higher switching loss of the power converter. The effect of different zero voltage vector selection schemes is verified by both simulation and experimental results for a 200-W salient-pole PMSM drive system.**

Keywords—direct torque control (DTC), duty ratio modulation (DRM), permanent-magnet synchronous motor (PMSM), pulse-width modulation (PWM), saturation controller, zero voltage vector selection.

I. Introduction

Direct torque control (DTC) was first proposed by Takahashi, Noguchi, and Depenbrock in the 1980s for induction motor (IM) drive systems [1], [2]. In the DTC method, according to the position of the stator flux and the errors between the reference and calculated values of the electromagnetic torque and stator flux, suitable voltage vectors are selected to control the stator flux and electromagnetic torque of the motor directly. Compared with the vector control method, the DTC has the advantages of fast torque response, simple implementation, etc. Because of these advantages, the DTC was soon applied to permanent-magnet synchronous motor (PMSM) drive systems in the 1990s [3]-[5].

In the conventional DTC-based PMSM drive systems, six nonzero voltage vectors are employed to control the electromagnetic torque and stator flux. This, however, generates problems such as torque ripples and nonconstant switching frequency which deteriorate the system performance. To solve these problems, several methods of using zero voltage vectors have been proposed for the DTC PMSM drive systems. One method is the space vector modulation-based DTC [6]-[8], where a voltage vector that would exactly compensate the errors of the torque and stator flux was calculated and synthesized by adjacent nonzero voltage vectors and two zero voltage vectors. This method can effectively reduce torque ripples but needs a complex calculation and the information of motor parameters.

Another method is the duty ratio modulation (DRM), which reduces both the torque and stator flux ripples [9]-[12]. In each sampling cycle, according to the duty ratio determined, appropriate nonzero voltage vectors are first selected and used during part of the cycle; and, then, appropriate zero voltage vectors are used during the rest of the cycle. The determination of the duty ratio for the nonzero voltage vector(s) is the key issue of the DRM method. Recently, a novel DRM DTC called DDTC was proposed in [10] to reduce both the stator flux and torque ripples by using the torque and stator flux slopes to determine the DRM. However, these DRM DTC methods also need motor parameters and have high computational costs. An adaptive saturation controller-based DRM DTC was proposed in [12], where both the signs and the magnitudes of the torque and stator flux errors were used to reduce the torque and stator flux ripples and eliminate the torque tracking errors in the steady state. However, only the zero voltage vector (000) was used in the switching table. The effect of using zero voltage vectors (000) and (111) on the performance of the torque and flux ripple reduction was not studied in [12].

The aim of this paper is to extend the work in [12] to study the effect of four different schemes of using the zero voltage vectors (000) and (111) on the torque and flux ripples, steady-state torque errors, total harmonic distortion (THD) of stator currents, and switching frequency of the adaptive saturation controller-based DRM DTC PMSM drive systems. The four schemes generate four different PWM waveforms, i.e., the three-voltage-vectors-based minimum discontinuous PWM (DPWMMIN), discontinuous PWM (DPWM), and maximum

This work was supported in part by the Nebraska Public Power District through the Nebraska Center for Energy Sciences Research.

discontinuous PWM (DPWMMAX), and the four-voltage-vectors-based continuous PWM (CPWM), in each control cycle of the DTC system. The performance of the four zero-voltage-vector-selection schemes is evaluated by simulation studies in MATLAB/Simulink and experimental studies on a 200-W salient-pole PMSM drive system. Results show that the CPWM scheme has lower torque ripple, less steady-state torque error, and lower stator current THD but a higher switching frequency than the DPWMMIN, DPWM, and DPWMMAX schemes.

II. Zero Voltage Vector Selection Schemes for a Saturation Controller-Based DTC PMSM Drive

A. The Saturation Controller-Based DTC System for a PMSM Drive

The schematic diagram of the saturation controller-based DTC system [12] for a PMSM drive is shown in Fig. 1, which consists of four parts: a torque and stator flux estimator, two saturation controllers, a hysteresis comparator, and a switching table. Based on the sector number determined by the location of the stator flux vector and the outputs s_T and s_ψ of the saturation controllers, a combination of multiple voltage vectors is selected from the switching table and then applied to the inverter to minimize the torque and flux errors. The two saturation controllers output not only the discrete state 0 or 1 but also continuous values between 0 and 1. This makes the voltage vector selection more flexible and avoids overusing the nonzero voltage vectors in one sampling period. In addition, an ancillary torque hysteresis comparator is designed to provide a supplementary signal c_T to judge when a sharp torque change is required to ensure a fast dynamic response of the DTC system. The execution time for zero voltage vectors is determined by the output of the torque saturation controller s_T. According to the values of s_T and s_ψ, the desired duty ratio vector of the inverter, d, can be modified as follows considering the two zero voltage vectors V_0 (000) and V_7 (111).

$$d = s_T\left(s_\psi \cdot v_{act1} + \left(1-s_\psi\right)\cdot v_{act2}\right) + \left(1-s_T\right)\left(\mu \cdot V_0 + (1-\mu)\cdot V_7\right) \quad \text{if } c_T = 1 \qquad (1)$$

$$d = (1-s_T)\left(s_\psi \cdot v_{act1} + \left(1-s_\psi\right)\cdot v_{act2}\right) + s_T\left(\mu \cdot V_0 + (1-\mu)\cdot V_7\right) \quad \text{if } c_T = 0 \qquad (2)$$

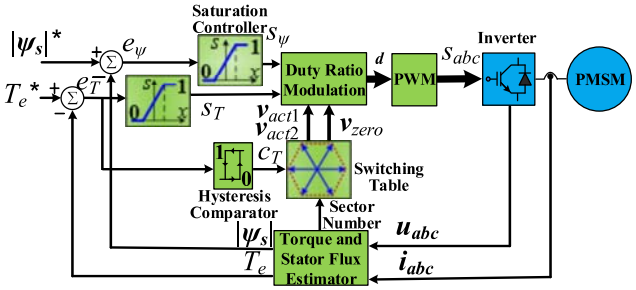

Fig. 1. The saturation controller-based DTC system for a PMSM drive.

where v_{act1} and v_{act2} are the two active (nonzero) voltage vectors; μ determines the weights of the two zero voltage vectors and can be a constant or a variable. The nonzero voltage vectors and two zero voltage vectors are selected from Table I and are in the same order as seen in the table. These voltage vectors are selected in each control cycle based on the position of the stator flux ψ_s in one of the six sectors and the torque comparator output c_T. The activation time of each selected voltage vector is equal to its coefficient in (1) (e.g., $s_T \cdot s_\psi$ for v_{act1}) or (2). In each switching cycle, (1) or (2) is executed when c_T is equal to 1 or 0, respectively.

B. Proposed Switching Table for the Saturation Controller-Based DTC with Four Zero Voltage Vector Selection Schemes

Table I shows the switching table of the saturation controller-based DTC system with four different schemes of using the two zero voltage vectors V_0 and V_7. The four schemes generate four different PWM waveforms in each control cycle, which are the three-voltage-vectors-based DPWMMIN (i.e., μ = 1), DPWMMAX (i.e., μ = 0), and DPWM (i.e., μ = 1 for Sectors 1, 3 and 5; μ = 0 for Sectors 2, 4 and 6), and the four-voltage-vectors-based CPWM (i.e., μ = 0.5). The DPWMMIN is the same as that used in [12], in which only the zero voltage vector V_0 is used. Each scheme in Table I outputs a combination of two nonzero voltage vectors and one or two zero voltage vectors, which are synthesized to generate the duty ratio for the inverter according to (1) or (2).

III. Effects of the Zero Voltage Vectors on Stator Flux and Torque

For a salient-pole PMSM, the stator flux vector $\psi_{s\alpha\beta}$ in the $\alpha\beta$ stationary reference frame is expressed by

$$\psi_{s\alpha\beta}(t) = \int \left(v_{s\alpha\beta}(t) - R_s i_{s\alpha\beta}(t)\right)dt \qquad (3)$$

where $v_{s\alpha\beta}$ and $i_{s\alpha\beta}$ are the stator voltage and current vectors in the stationary reference frame, respectively; and R_s is the

TABLE I:
Switching Table of the Saturation Controller-Based DTC with Four Different Zero Voltage Vector Selection Schemes.

Sector	1	2	3	4	5	6	PWM Patterns
$c_T = 1$	V_2(110)	V_3(010)	V_4(011)	V_5(001)	V_6(101)	V_1(100)	Nonzero Vectors
	V_3(010)	V_4(011)	V_5(001)	V_6(101)	V_1(100)	V_2(110)	
	V_0(000)	V_0(000)	V_0(000)	V_0(000)	V_0(000)	V_0(000)	DPWMMIN
	V_0(000)	V_7(111)	V_0(000)	V_7(111)	V_0(000)	V_7(111)	DPWM
	V_7(111)	V_7(111)	V_7(111)	V_7(111)	V_7(111)	V_7(111)	DPWMMAX
	V_0(000)	V_0(000)	V_0(000)	V_0(000)	V_0(000)	V_0(000)	CPWM
	V_7(111)	V_7(111)	V_7(111)	V_7(111)	V_7(111)	V_7(111)	
$c_T = 0$	V_6(101)	V_1(100)	V_2(110)	V_3(010)	V_4(011)	V_5(001)	Nonzero Vectors
	V_5(001)	V_6(101)	V_1(100)	V_2(110)	V_3(010)	V_4(011)	
	V_0(000)	V_0(000)	V_0(000)	V_0(000)	V_0(000)	V_0(000)	DPWMMIN
	V_0(000)	V_7(111)	V_0(000)	V_7(111)	V_0(000)	V_7(111)	DPWM
	V_7(111)	V_7(111)	V_7(111)	V_7(111)	V_7(111)	V_7(111)	DPWMMAX
	V_0(000)	V_0(000)	V_0(000)	V_0(000)	V_0(000)	V_0(000)	CPWM
	V_7(111)	V_7(111)	V_7(111)	V_7(111)	V_7(111)	V_7(111)	

stator armature resistance.

Neglecting the voltage drop on the stator resistance, (3) can be expressed in the discrete-time format as follows.

$$\psi_{s\alpha\beta}(t)\big|_{t=T_s} = v_{s\alpha\beta}(t)\big|_{t=0} \cdot T_s + \psi_{s\alpha\beta}(t)\big|_{t=0} \tag{4}$$

where T_s is the switching period. If zero voltage vector(s) are used, the stator flux vector will remain constant, meaning that both the angular position and the amplitude of the stator flux vector remain unchanged. Then, the change of the load angle, $\Delta\delta$, can be evaluated by

$$\Delta\delta = \Delta\theta_{(VT)} - \omega_e T_s = -\omega_e T_s \tag{5}$$

where $\Delta\theta_{(VT)}$ is the change of the angular position of the stator flux vector and ω_e is rotor electrical angular speed.

Assume that the stator flux vector lies in Sector 1. The effect of the zero voltage vectors on the stator flux is illustrated in Fig. 2, where $\psi_{r\alpha\beta}(t)$ and $\psi_{r\alpha\beta}(t+T_s)$ are the rotor flux vector at time t and $t+T_s$ in the $\alpha\beta$ stationary reference frame, respectively. The dynamic equations of the salient-pole PMSM in the rotor reference frame can be written as follows.

$$\begin{bmatrix} v_{sd} \\ v_{sq} \end{bmatrix} = \begin{bmatrix} R_s + pL_d & -\omega_e L_q \\ \omega_e L_d & R_s + pL_q \end{bmatrix} \begin{bmatrix} i_{sd} \\ i_{sq} \end{bmatrix} + \begin{bmatrix} 0 \\ \omega_e \psi_m \end{bmatrix} \tag{6}$$

$$T_e = \frac{3}{2} n \cdot \psi_m \cdot i_{sq} + \frac{3}{2} n \left(L_d - L_q \right) i_{sd} \cdot i_{sq} \tag{7}$$

where v_{sd} and v_{sq} are the d- and q-axis stator voltages, respectively; i_{sd} and i_{sq} are the d- and q-axis stator currents, respectively; L_d and L_q are the d- and q-axis inductances, respectively; ψ_m is rotor magnet flux linkage; $p = d/dt$ is the time derivative operator; T_e is the electromagnetic torque; and n is the number of pole pairs.

The d- and q-axis stator flux linkages, ψ_{sd} and ψ_{sq}, can be expressed as

$$\begin{bmatrix} \psi_{sd} \\ \psi_{sq} \end{bmatrix} = \begin{bmatrix} L_d & 0 \\ 0 & L_q \end{bmatrix} \begin{bmatrix} i_{sd} \\ i_{sq} \end{bmatrix} + \begin{bmatrix} \psi_m \\ 0 \end{bmatrix} \tag{8}$$

According to (8), (7) can be rewritten as follows.

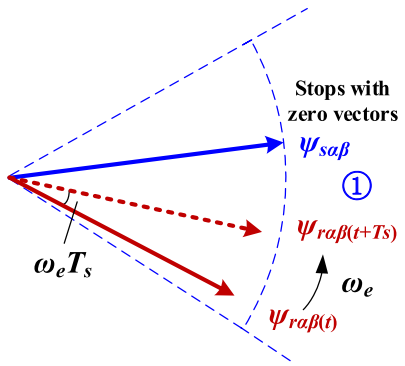

Fig. 2. Effect of the zero voltage vectors on the stator flux vector.

$$T_e = \frac{3}{2}\frac{n}{L_d}|\psi_s|\psi_m \sin\delta + \frac{3}{4}\frac{n}{L_d L_q}|\psi_s|^2 \left(L_d - L_q\right)\sin(2\delta) \tag{9}$$

where δ is the load angle and $|\psi_s|$ is the magnitude of the stator flux vector.

Taking the derivative of (9) with respect to time yields

$$\begin{aligned} \frac{dT_e}{dt} = {} & \frac{3}{2}\frac{n}{L_d}\left[\psi_m \sin\delta - \frac{L_q - L_d}{L_q}|\psi_s|\sin(2\delta)\right] \times \frac{d|\psi_s|}{dt} \\ & + \frac{3}{2}\frac{n}{L_d}\left[|\psi_s|\psi_m \cos\delta - \frac{L_q - L_d}{L_q}|\psi_s|^2 \cos(2\delta)\right] \times \frac{d\delta}{dt} \end{aligned} \tag{10}$$

By discretizing (10), the torque variation can be expressed as

$$\begin{aligned} \Delta T_e = {} & \frac{3}{2}\frac{n}{L_d}\left[\psi_m \sin\delta_0 - \frac{L_q - L_d}{L_q}|\psi_s|_0 \sin(2\delta_0)\right] \times \Delta|\psi_s| \\ & + \frac{3}{2}\frac{n}{L_d}\left[|\psi_s|_0 \psi_m \cos\delta_0 - \frac{L_q - L_d}{L_q}|\psi_s|_0^2 \cos(2\delta_0)\right] \times \Delta\delta \end{aligned} \tag{11}$$

where $|\psi_s|_0$ and δ_0 are the stator flux magnitude and the load angle at the reference point, respectively; and $|\Delta\psi_s|$ is the change of stator flux magnitude.

Since the use of zero voltage vectors (000) and/or (111) will not change the position or magnitude of the stator flux vector, the torque variation is only related to the load angle variation. According to (5), when using zero voltage vectors, the change of the load angle is proportional to the switching period. Therefore, the torque variation is proportional to the switching period. By using the four zero voltage selection schemes, different switching periods can be generated to reduce the torque variation.

IV. Simulation Results

Simulation studies were carried out in MATLAB/Simulink to evaluate the saturation controller-based DTC system with the proposed four different zero voltage vector selection schemes for a 200-W salient-pole PMSM drive system. The parameters of the PMSM are given as follows. The maximum speed is 3000 rpm; R_s = 0.235 Ω; L_d = 0.275 mH; L_q = 0.364 mH; the voltage constant K_e = 9.7 V/krpm; the number of pole pairs is n = 4; and the momentum of inertia is J = 0.000007 kg·m^2. The DC bus voltage of the inverter is 41.75 V. The sampling frequency is 10 kHz. The boundaries of the torque and stator flux saturation functions and the hysteresis comparator are 0.3 N·m and 0.003 V·s, respectively.

The steady-state performances of the four zero voltage vector selection schemes were compared for the PMSM operating at 1500 rpm, where the commands of the torque and the stator flux magnitude were 0.5 N·m and 0.0135 V·s, respectively. The stator current, torque magnitude, and duty ratio of the system using the four zero voltage vector selection schemes are compared in Fig. 3. The steady-state torque error,

torque ripples, THD of stator phase current, and switching frequency of the four schemes are compared in Table II. The average switching frequency, f_{av}, is calculated by $f_{av} = N_T/T$, where N_T is the total number of switching times of one IGBT switch of the inverter during a fixed period T, which is 0.01 s in the simulation. The results show that the CPWM achieves the lowest torque ripple, least steady-state torque error, and lowest stator current THD. However, the switching frequency of the CPWM is higher than the other three schemes, but is acceptable in the real control system.

Fig. 4 shows the simulation results of the steady-state performance of the CPWM using different weights for the two zero voltage vectors when the rotor speed is 1500 rpm and the load is 0.5 N·m. It is clear that when the weight μ is 0.5, the CPWM can get the best steady-state performance, i.e.,

TABLE II:
Steady-State Performance of the Four Zero Voltage Vector Selection Schemes.

Performance metric	DPWMMIN	DPWM	DPWMMAX	CPWM
Steady-state torque error (N·m)	0.0080	0.0132	0.0073	0.0057
Torque ripple (N·m)	0.0280	0.0337	0.0304	0.0134
THD of stator phase current (%)	5.82	5.64	4.86	3.45
f_{av} (kHz)	6.7	6.7	6.7	10

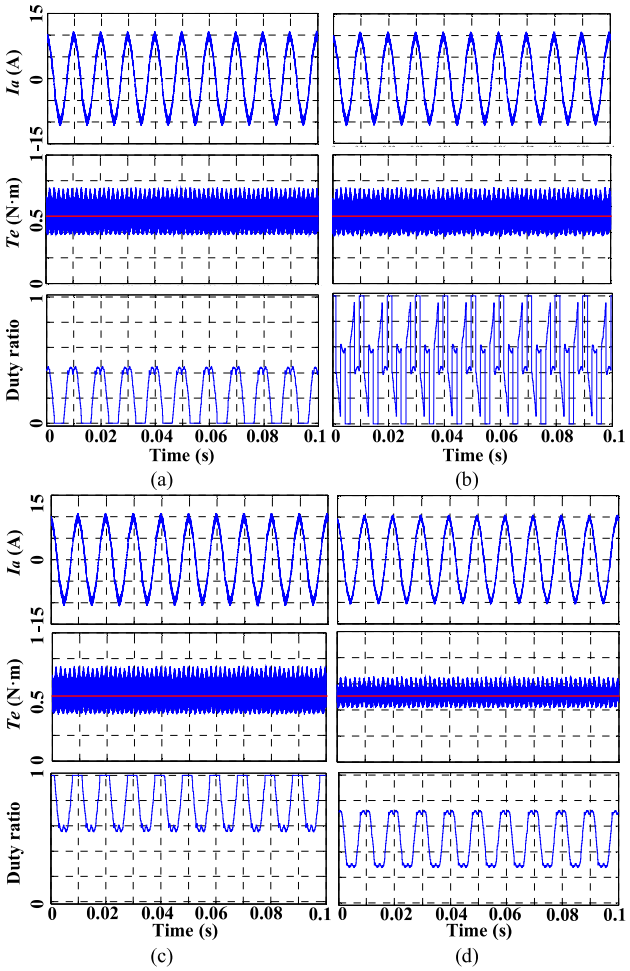

Fig. 3. Simulation results of the steady-state performance of the four methods: (a) DPWMMIN, (b) DPWM, (c) DPWMMAX, and (d) CPWM.

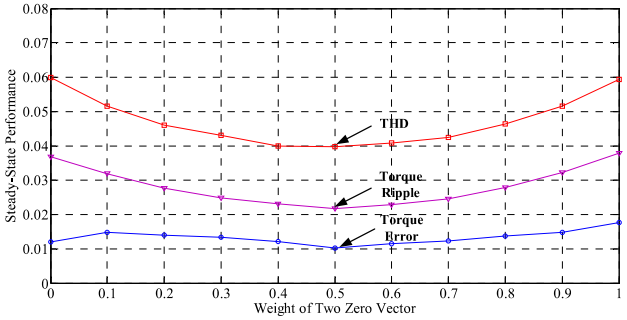

Fig. 4. Steady-state performance of the CPWM using different weights of the two zero voltage vectors.

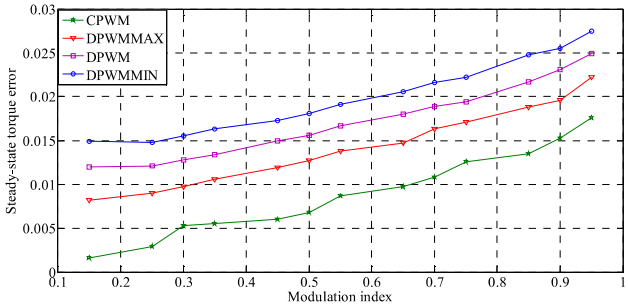

Fig. 5. Steady-state torque errors of the four PWM schemes at different modulation indexes.

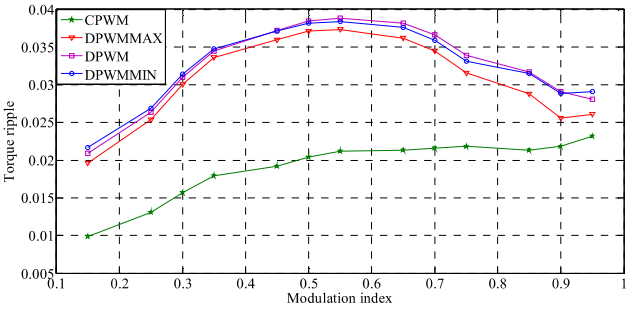

Fig. 6. Steady-state torque ripples of the four PWM schemes at different modulation indexes.

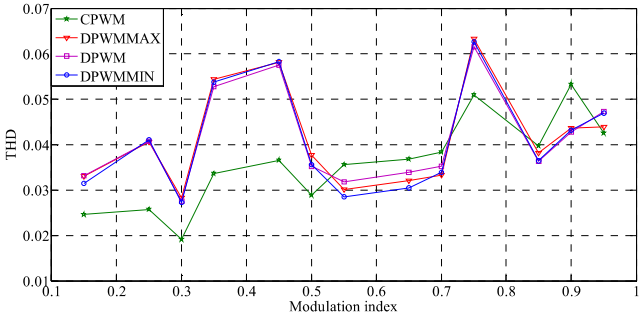

Fig. 7. Stator phase current THDs of the four PWM schemes at different modulation indexes.

minimum steady-state torque error, harmonic torque ripple, and stator phase current THD. Figs. 5-7 show the steady-state simulation results of the four PWM schemes using different modulation indexes when the weight of the two zero voltage vectors is 0.5, the rotor speed is 1500 rpm, and the load is 0.5 N·m. It can be seen that as the modulation index increases, the steady-state torque error becomes larger and larger for the four methods. The CPWM achieves the smallest torque error during the whole range of the rotor speed. The steady-state torque ripples when using the DPWMMAX, DPWM, and DPWMMIN are quite close at the same modulation index and are all larger than that when using the CPWM. Among the four schemes, the CPWM has the smallest average stator current THD during the whole range of the modulation index.

V. Experimental Results

Experimental studies were carried out to further evaluate the four zero voltage vector selection schemes for the 200-W PMSM drive system used in the simulation studies. The control algorithms were implemented in a dSPACE 1104 real-time control system with a sampling period of 100 μs. The dead time was set as 1 μs. The hardware setup of the experimental system is shown in Fig. 8. Experiments were performed on the system at the same operating condition evaluated in the simulation study in Section IV, and the results are compared in Fig. 9 and Table III. The CPWM achieves the best performance in terms of the torque ripple, steady-state torque error, and stator current THD, but has a higher switching frequency than the other three schemes. The experimental results agree with the simulation results.

VI. Conclusion

This paper has investigated the effect of four different zero voltage vector selection schemes on the performance of a salient-pole PMSM drive system using a saturation controller-based DTC. The four zero voltage vector selection schemes led to four different PWM generation schemes, which are the three-voltage-vectors-based DPWMMIN, DPWM, and DPWMMAX, and the four-voltage-vectors-based CPWM. Compared to the other three schemes, the CPWM enabled the DTC system to achieve the lowest torque ripple, steady-state torque error, and stator current THD at a cost of a 50% increase of the switching frequency. This has been verified by simulation and experimental results on a 200-W salient-pole PMSM system.

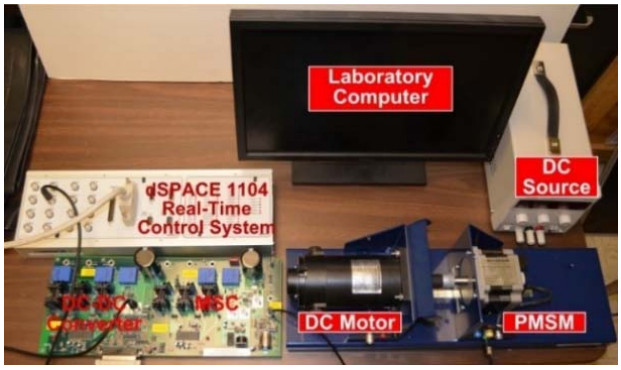

Fig. 8. The experimental system setup.

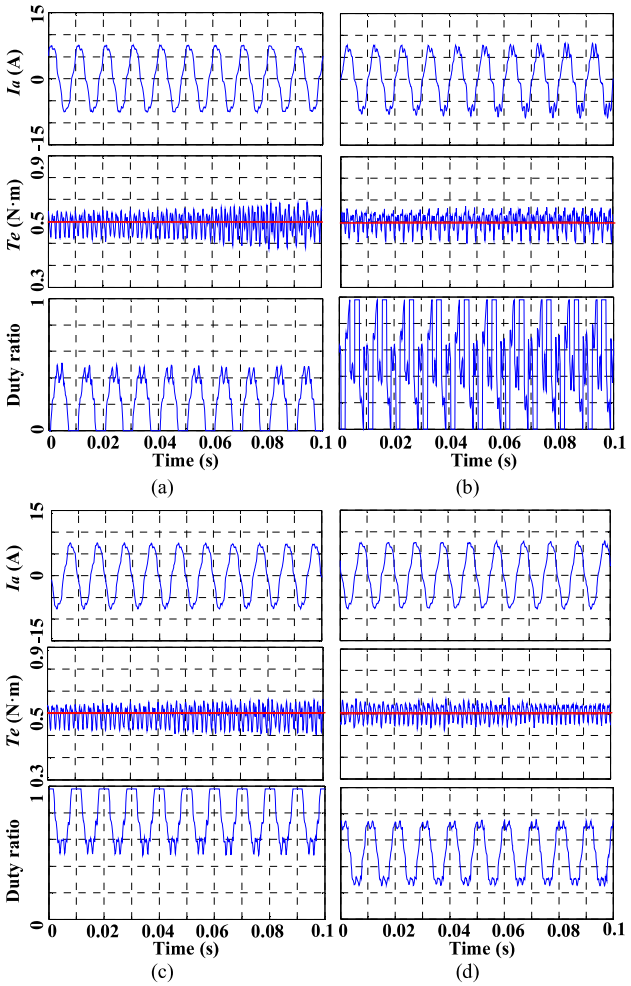

Fig. 9. Experimental results of the steady-state performance of the four schemes: (a) DPWMMIN, (b) DPWM, (c) DPWMMAX, and (d) CPWM.

TABLE III:
Steady-State Performance of the Four Zero Voltage Vector Selection Schemes.

Performance metric	DPWMMIN	DPWM	DPWMMAX	CPWM
Steady-state torque error (N·m)	0.0220	0.0198	0.0212	0.0102
Torque ripple (N·m)	0.0391	0.0390	0.0412	0.0217
THD of stator phase current (%)	6.00	5.91	5.95	3.98
f_{av} (kHz)	6.7	6.7	6.7	10

References

[1] I. Takahashi and T. Naguchi, "A new quick-response and high-efficiency control strategy of an induction motor," *IEEE Trans. Ind. Appl.*, vol. 22, pp. 820-827, Sept./Oct. 1986.

[2] M. Depenbrock, "Direct self-control (DSC) of inverter-fed induction machine," *IEEE Trans. Power Electron.*, vol. 3, no. 4, pp. 420-429, Oct. 1988.

[3] C. French and P. Acarnley, "Direct torque control of permanent magnet drives," *IEEE Trans. Ind. Appl.*, vol. 32, pp. 1080-1088, Sept./Oct. 1996.

[4] L. Zhong, M. Rahman, W. Hu, and K. Lim, "Analysis of direct torque control in permanent magnet synchronous motor systems," *IEEE Trans. Power Electron.*, vol. 12, no. 3, pp. 528-536, May 1997.

[5] G. Buja and M. Kazmierkowski, "Direct torque control of PWM inverter-fed AC motors-a survey," *IEEE Trans. Ind. Electron.*, vol. 51, pp. 741-757, 2004.

[6] G. Foo and M. Rahman, "Sensorless direct torque and flux-controlled IPM synchronous motor drive at very low speed without signal injection," *IEEE Trans. Ind. Electron.*, vol. 57, no. 1, pp. 395-403, Jan. 2010.

[7] Y. Zhang, J. Zhu, W. Xu, and Y. Guo, "A simple method to reduce torque ripple in direct torque-controlled permanent-magnet synchronous motor by using vectors with variable amplitude and angle," *IEEE Trans. Ind. Electron.*, vol. 58, no. 7, pp. 2848-2859, Jul. 2011.

[8] A. H. Abosh, Z. Zhu, and Y. Ren, "Reduction of torque and flux ripples in space vector modulation-based direct torque control of asymmetric permanent magnet synchronous machine," *IEEE Trans. Power Electron.*, vol. 32, no. 4, pp. 2976-2986, Apr. 2017.

[9] D. Mohan, X. Zhang, and G. H. B. Foo, "A simple duty cycle control strategy to reduce torque ripples and improve low-speed performance of a three-level inverter fed DTC IPMSM drive," *IEEE Trans. Ind. Electron.*, vol. 64, no. 4, pp. 2709-2721, Apr. 2017.

[10] Y. Ren, Z. Q. Zhu, and J. Liu, "Direct torque control of permanent-magnet synchronous machine drives with a simple duty ratio regulator," *IEEE Trans. Ind. Electron.*, vol. 61, no. 10, pp. 5249-5258, Oct. 2014.

[11] F. Niu, K. Li, and Y. Wang, "Direct torque control for permanent-magnet synchronous machines based on duty ratio modulation," *IEEE Trans. Ind. Electron.,* vol. 62, no. 10, pp. 6160-6170, Oct. 2015.

[12] Z. Zhang, C. Wei, W. Qiao, and L. Qu, "Adaptive saturation controller-based direct torque control for permanent-magnet synchronous machines," *IEEE Trans. Power Electron.*, vol. 31, no. 10, pp. 7112-7122, Oct. 2016.